IOP Publishing Superconductor Science and Technology
Supercond. Sci. Technol. 30 (2017) 064004 (10pp) https://doi.org/10.1088/1361-6668/aa684f

Engineering of second generation HTS coated conductor architecture to enhance the normal zone propagation velocity in various operating conditions

C Lacroix, F Sirois and J-H Fournier Lupien

Department of Electrical Engineering, Polytechnique Montréal, Montréal, QC, H3C 3A7, Canada

E-mail: christian.lacroix@polymtl.ca

Received 19 December 2016, revised 10 March 2017
Accepted for publication 22 March 2017
Published 11 May 2017

Abstract

The effects of operating conditions, critical current and stabilizer geometry on the normal zone propagation velocity (NZPV) of second generation (2G) high-temperature superconductor (HTS) coated conductors (CCs) are investigated using finite element simulations. The NZPV of tapes with a low interfacial resistance between the HTS and stabilizer layers are first compared with tapes with a current flow diverter (CFD) architecture. Our results indicates that the CFD concept increases the NZPV for the whole range of operating temperatures investigated (10–77 K). In particular, for an operating temperature of 77 K and an operating current of $0.9I_c$, our numerical results indicate that the NZPV of a 2G HTS CC with a CFD architecture and a 2 μm thick stabilizer layer could reach a value of 50 m s^{-1}. Furthermore, numerical simulations realized on the effect of the stabilizer geometry on the NZPV of 2G HTS CCs revealed that putting most of the stabilizer on the substrate side can enhance the NZPV by a factor of 7 or more, even for tape with thick stabilizer (20 μm or more). This is particularly promising for improving quench detection in applications requiring a thick stabilizer such as superconducting coils.

Keywords: coated conductors, quench, normal zone propagation velocity, hot spot, high-temperature superconductor

(Some figures may appear in colour only in the online journal)

1. Introduction

Present commercial superconducting tapes based on (RE)BaCuO, also called second generation (2G) high-temperature superconductor (HTS) coated conductors (CCs), show remarkable electrical and mechanical properties and are currently used in many large scale projects. One important aspect to consider when designing superconducting devices is the protection of the device when a quench occurs. Quench dynamics of 2G HTS CCs has been investigated by several groups over the years, both experimentally [1–6] and by numerical simulations [7–11]. A crucial issue that needs to be resolved is the low normal zone propagation velocity (NZPV) in those (RE)BaCuO-based tapes in comparison to low-temperature superconducting wires. A low NZPV increases the probability to develop destructive hot spots when an inhomogeneous quench occurs, which is likely to happen when the operating current I_{op} is close to the critical current I_c.

The common approach used by tape manufacturers to mitigate the chance of developing hot spots is to significantly increase the thickness of the metallic sheath (often called the stabilizer). However, this approach has the drawback of reducing the engineering critical current density, which is undesirable for coils applications [12]. Similarly, a thicker stabilizer reduces the resistance per unit length when the HTS is in the normal state, which is undesirable for current limiter applications [13].

Another solution to the hot spot problem is to modify the tape architecture in order to increase the NZPV. Having a faster normal zone propagation makes the quench more uniform and, as a consequence, accelerates the increase of the HTS tape

resistance just after the appearance of a local normal zone. In the case of coil applications, this translates into faster quench detection and thus better protection of the device [1, 14]. Furthermore, increasing the NZPV would allow reducing the stabilizer thickness of HTS tapes used in a resistive-type superconducting fault current limiter (SFCL) [15], which would be beneficial in terms of performance, reliability and cost.

It has been shown theoretically and experimentally that the NZPV could be significantly increased in 2G HTS CCs in presence of a high interfacial electrical resistance between the HTS and the stabilizer [16, 17]. More recently, the current flow diverter (CFD) concept was proposed to enhance the NZPV of 2G HTS CCs [18]. The key point of the CFD concept is to increase the current transfer length (CTL), which is the length over which the current transfers from the HTS to the stabilizer (or from the stabilizer to the HTS). In [18], it was proposed to integrate a high resistive layer at the HTS-stabilizer interface, but to keep a low interfacial resistance on the edges of the tape. Numerical simulations demonstrated that this concept allows increasing the NZPV while keeping the overall interfacial resistance at acceptable values. The CFD concept was afterwards realized experimentally using modified commercial tapes [19].

Up to now, the enhanced NZPV using the CFD concept have been only demonstrated for a single set of parameters, namely an operating temperature of 77 K, a stabilizer thickness of $\approx$2–3 μm and a critical current density $\approx 2.5 \times 10^{10}\,\mathrm{A\,m^{-2}}$. Therefore, it is relevant to investigate the effects of the operating conditions, the critical current and the stabilizer thickness on the NZPV of various HTS tape architectures. In this work, we used finite element simulations to evaluate quantitatively the effects of these parameters for HTS tapes in which a high resistance layer is inserted at the center of the HTS-stabilizer interface while keeping a low interfacial resistance on the tape edges (CFD architecture). We also investigated how the stabilizer located on the *substrate side* and on the *lateral edges* of the tape influences the NZPV.

2. Finite element electrothermal model

The 3D finite element simulations were realized with the help of the Joule heating module of the COMSOL Multiphysics 4.3b software package. The following materials were used in the simulations: Ag as the stabilizer, MgO as the buffer layers, (RE)BaCuO as the HTS layer and Hastelloy as the substrate. Most of the physical parameters of the materials used in the simulations can be found in the literature (see references provided in [18]). In the case of (RE)BaCuO ($T < T_c$), its electrical conductivity was approximated by using a power-law model in the flux creep and flux flow regimes (σ_{sc}) while the transition from the superconducting state to the normal state (σ_n) was modeled assuming two resistances in parallel.

Based on experimental data found in literature [3, 20–22], the following equations were used:

$$\sigma_{\mathrm{REBCO}}(T) = \sigma_{sc}(T) + \sigma_n(T), \tag{1}$$

$$\sigma_{sc}(T) = \frac{J_c(T)}{E_0}\left(\frac{\|E\|}{E_0}\right)^{\frac{1-n(T)}{n(T)}}, \tag{2}$$

Table 1. (RE)BaCuO model parameters ($T_0 = 50$ K).

Parameter	Numerical value
J_{c0} (critical current density at $T = T_0$)	8.0 MA cm^{-2}
T_c (critical temperature)	90 K
E_0 (electric field criterion)	1 μV cm^{-2}
n_0 (n-parameter at $T = T_0$)	20

$$J_c(T) = \begin{cases} J_{c0}\left(\frac{T_c - T}{T_c - T_0}\right) & \text{for } T < T_c \\ 0 & \text{for } T \geqslant T_c \end{cases}, \tag{3}$$

$$n(T) = \begin{cases} (n_0 - 10)\left(\frac{T_c - T}{T_c - T_0}\right) + 10 & \text{for } T < T_c \\ 1 & \text{for } T \geqslant T_c \end{cases}, \tag{4}$$

where T_0 is an arbitrary temperature below T_c (here, we chose $T_0 = 50$ K), J_{c0} is the critical current density at T_0, T_c is the critical temperature, $\|E\|$ is the norm of the electric field, E_0 is the electric field criterion and n_0 is a fitting parameter. The values for each parameter are provided in table 1.

The variables used in the electro-thermal model are the electric potential V and the temperature T. These two variables are calculated using the current continuity equation and the heat equation respectively, as described in details in [18]. A current $I(t)$ is imposed at one end of the tape (S_1 in figure 1(c)) while the other end (S_2 in figure 1(c)) is grounded. Also, we consider the system to be adiabatic, i.e. no heat is exchanged with the surrounding environment.

To minimize computation time of this 3D numerical model, the number of elements was reduced by taking advantage of the symmetries of the problem, i.e. only half of the tape width was modeled. Also, the region where the heat is deposited to create a normal zone was placed at one end of the tape, while the current was injected at the other end. To further reduce the computation time, the buffer layers and the interfacial layer were approximated as 2D domains, i.e. as if they were infinitely thin (see [18] for further details).

3. Determination of the NZPV

The reference tape architecture is presented in figure 1(a). It consists of a stabilizer layer (gray), a HTS layer (white) and buffer layers (yellow) deposited on a substrate (brown). The interfacial layer between the HTS and the stabilizer is also included in the drawing (green). The black arrow represents a virtual probe. The geometrical parameters used for the reference architecture in the simulations are presented in table 2.

The cross-section of a tape with a 'CFD' architecture [18], abbreviated 'CFD', is shown in figure 1(b). The only difference with the reference architecture is that a layer of high electrical resistance (blue) is inserted at the HTS-stabilizer interface. This high electrical resistance layer covers only partially the interface (middle part of the tape). The resistance of the remaining interfaces (green) remains low. The parameters used for the CFD architecture in the simulations are also presented in table 2.

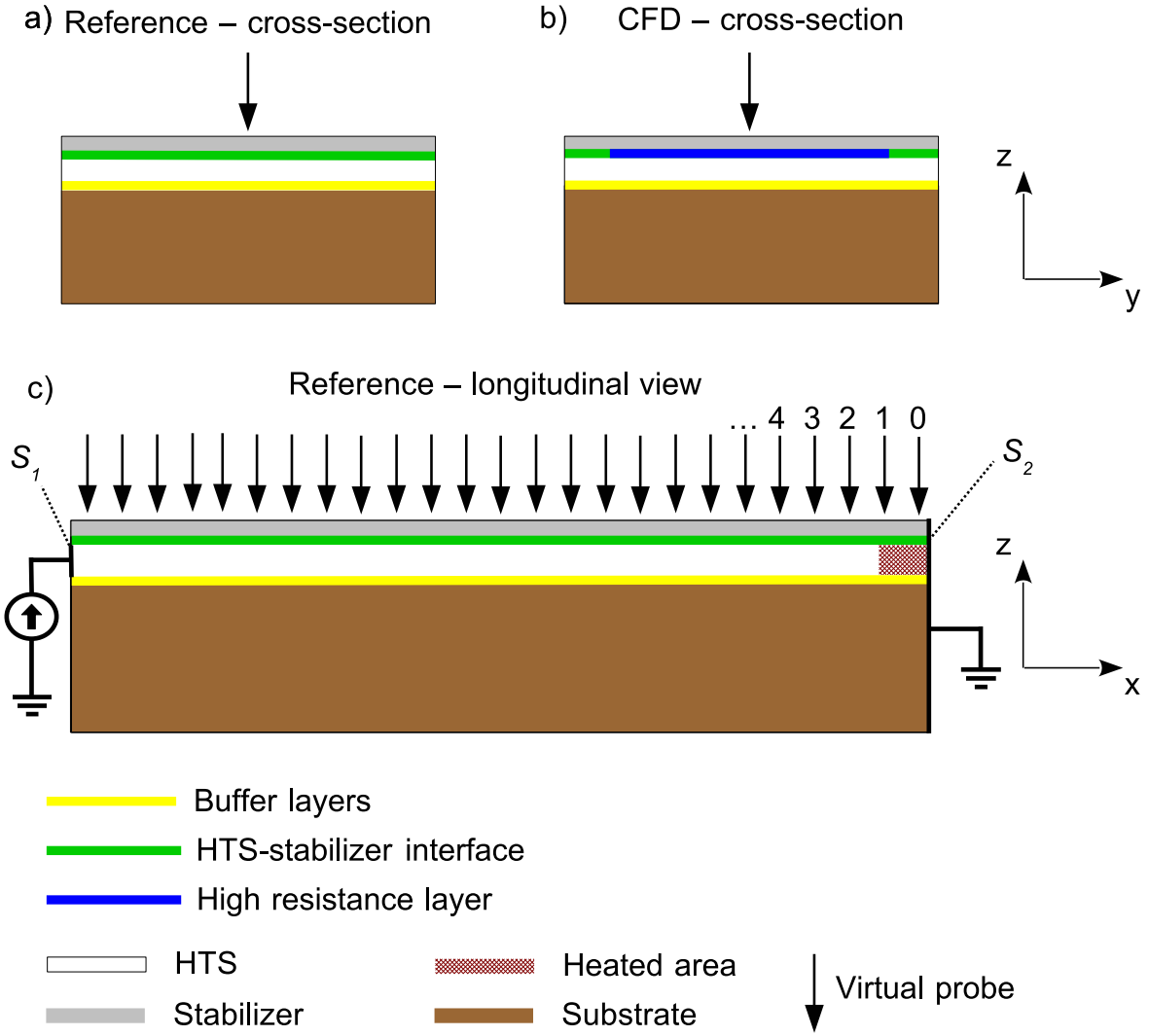

Figure 1. Tape geometries used in finite element simulations (not at scale): (a) cross-section view of the reference architecture, (b) cross-section view of a CFD architecture and (c) longitudinal view of the reference architecture with a region (red) where heat is deposited to create a hot spot. The numbers are used to distinguish the virtual probes.

Table 2. Geometrical parameters of the simulated tapes. The colors correspond to those used in figures 1 and 8.

Parameter	Numerical value
Length of tape	5 cm
Width of tape	1 cm
Substrate thickness (brown)	50 μm
Buffer layers thickness (yellow)	150 nm
HTS layer thickness (white)	1 μm
HTS-Ag interfacial layer thickness (green)	100 nm[a]
High resistance layer (CFD) thickness (blue)	100 nm[a]
Width of high resistance layer (blue)	0.9 cm
Total stabilizer thickness (gray)	1–40 μm

[a] Modeled as infinitely thin layers in the finite elements simulations.

It is worth emphasizing that in the tape architectures illustrated in figures 1(a) and (b), there is no silver on the substrate side nor on the sides of the tape. As will be discussed later in section 5, the stabilizer geometry can affect significantly the NZPV. Therefore, in order to evaluate correctly the effect of a highly resistive layer at the HTS-stabilizer interface, we made sure to eliminate any effect due to the stabilizer geometry by using these tape architectures.

In figure 1(c), the longitudinal section of the reference architecture is shown. At one end of the tape, a current is imposed in the HTS layer while the other end is grounded. A series of probe (black arrows) were placed at every millimeter along the center of the tape. A ramp of current followed by a plateau of constant current corresponding to the operating current $I_{op} = 0.9I_c$, where I_c is the critical current, is imposed as transport current $I(t)$ in the tape (see figure 2). After the current just reaches the plateau, some amount of heat $Q(t)$ (in W m^{-3}) is deposited in the HTS layer at one end of the tape (red region in figure 1(c)) to create a normal zone. For each simulation, the value of Q_0 was adjusted approximately to the minimum value required to create a normal zone. The length d of the heated region is 1 mm and the heat impulse lasts 0.5 ms (see figure 2).

An example of the time evolution of the temperature during a quench is shown in figure 3 for a tape with a CFD

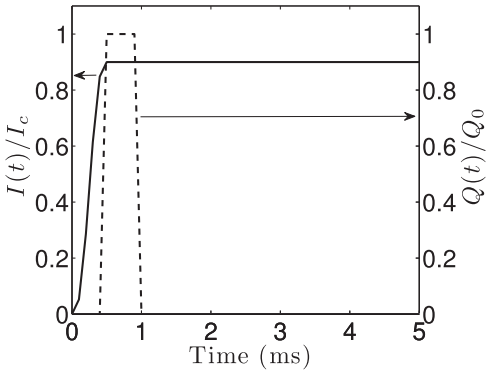

Figure 2. Left axis: waveform of the applied current $I(t)$ normalized by I_c as a function of time used in all simulations (solid line), where I_c is the critical current of the tape. Right axis: waveform of the heat impulse $Q(t)$ normalized by Q_0 used to create a normal zone (dashed line), where Q_0 is adjusted approximately to the minimum value required to create a normal zone.

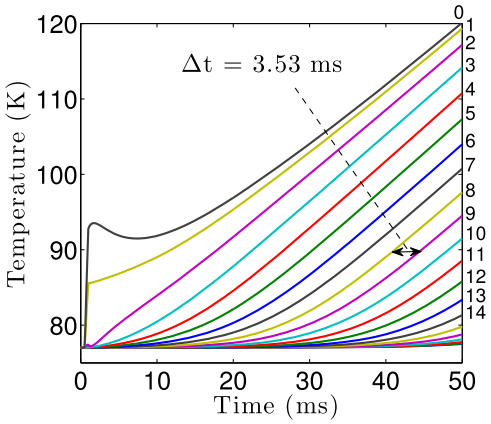

Figure 3. Time evolution of the temperature in a tape with the CFD architecture measured with the virtual probes located on top of the stabilizer layer, along the center line of the tape, as shown in figure 1(c). Each line represents the temperature measured by one virtual probe. The numbers on the right side of the graph indicate the position of each virtual probe as described in figure 1(c). The distance between each virtual probe is 1 mm. Here, the stabilizer thickness is 20 μm, the operating (initial) temperature is 77 K ($I_c = 260$ A) and the operating current is 234 A ($I_{op} = 0.9I_c$).

architecture. In this simulation, the stabilizer thickness is 20 microns, the operating (initial) temperature $T_{op} = 77$ K ($I_c = 260$ A) and the operating current $I_{op} = 0.9I_c = 234$ A. We observe that the temperature first rises at the location where the heat is deposited. When the temperature reaches 90 K, a normal zone appears and expands. The NZPV can then be calculated by dividing the distance between two virtual probes by the time elapsed to reach 90 K. In figure 3, the time elapsed is 3.53 ms between probes #8 and #9. Considering that the distance between the two probes is 1 mm, we obtain in this case a NZPV of 0.283 m s^{-1}.

In figure 4, we present the calculated NZPV between two successive probes located at different distances from the end of the tape where the heat is deposited. We observe that the NZPV values measured just besides the initial normal zone is lower than those measured far away from the initial normal zone. Furthermore, the NZPV values measured using probes far away

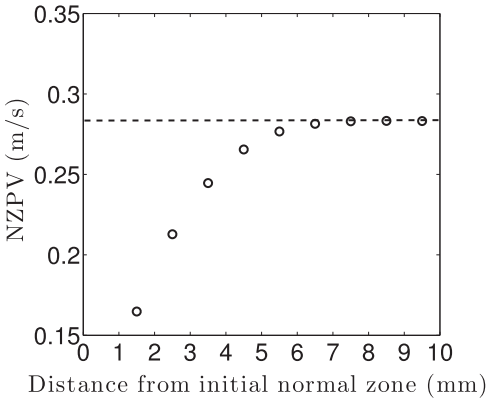

Figure 4. NZPV values obtained from figure 3 for different distances from the position of the initial normal zone, which corresponds to one end of the tape. The dashed line corresponds to the asymptotic value.

are the same if they are located at a sufficiently large distance from the initial normal zone location. This demonstrates that, when determining the NZPV, one must be careful to measure the NZPV at a location where it has reached its asymptotic value. A way to do this is to minimize the distance between each probe and to perform simulations on long tapes. However, this has the drawback of increasing the number of elements required in the simulation, and thus the computation time. Therefore, there is a trade-off to be made in order to get precise values of NZPV while maintaining reasonable computation times. It is worth mentioning that the NZPV can also be overestimated if too much heat is deposited at the location where the initial normal zone is created. In that case, the NZPV value is higher close to the initial normal zone and the calculated values diminishes gradually as we observe farther away from the initial normal zone to eventually reach an asymptotic value. Finally, it is important to set the appropriate number of elements in order to limit the error on the NZPV values obtained. For example, the NZPV can be over(under)estimated if the resolution of elements along the length of the tape is not sufficient [23].

4. Parametric study of the NZPV

In this section, we explore the NZPV of tapes with the reference architecture and the CFD architecture for different stabilizer thicknesses, critical current levels and operating temperatures. Simulations were carried out on tapes having the same overall HTS-stabilizer interfacial resistance $R_i = 1\ \mu\Omega\,\text{cm}^2$. In the case of tapes with the reference architecture, we considered that the HTS-stabilizer interface (green line in figure 1(a)) had a thickness of 100 nm and a conductivity of 10^3 S m^{-1}, which gives an interfacial resistance $R_i = 1\ \mu\Omega\,\text{cm}^2$. For tapes with the CFD architecture, the low resistance part of the interfacial layer (green line in figure 1(b)) was set to a constant value of $R_i^* = 0.1\ \mu\Omega\,\text{cm}^2$, which corresponds to a conductivity value of 10^4 S m^{-1} for a thickness of 100 nm. For the high resistance part of the HTS-stabilizer interfacial layer (blue line in figure 1(b)), simulations were realized using a thickness of 100 nm and a conductivity of 10^{-3} S m^{-1}, which corresponds to an interfacial resistance $R_f = 1\ \Omega\,\text{cm}^2$.

In the case where $R_f \gg R_i^*$, the resulting interfacial resistance is given by

$$R_i \approx \frac{R_i^*}{(1-f)}, \tag{5}$$

where $R_i^* = 0.1\ \mu\Omega\,\mathrm{cm}^2$, $f = w_f/w_t$ is the coverage fraction of the high resistance layer at the HTS-stabilizer interface, w_f is the width of the high resistance layer and w_t is the total width of the tape. For our simulations, the high resistance layer covered 90% of the width of the tape ($f = 0.9$), which finally gives $R_i \approx 1\ \mu\Omega\,\mathrm{cm}^2$ for a tape with the CFD architecture. Hence, both the reference and the CFD architectures considered here have the same global interfacial resistance of $1\ \mu\Omega\,\mathrm{cm}^2$, which somewhat normalizes the comparison.

4.1. Effect of stabilizer thickness

The thickness of the stabilizer (t_s) was varied in order to investigate its effect on the NZPV. Here, we first considered a tape with the reference architecture having a critical current of 260 A and operating at 77 K and 234 A. We observe from figure 5(a) (blue squares) that the NZPV varies from $0.08\ \mathrm{m\,s^{-1}}$ when $t_s = 20\ \mu$m to $0.47\ \mathrm{m\,s^{-1}}$ when $t_s = 1\ \mu$m. The dashed blue line is a fit of the data obtained with two power-law functions ($y = ax^b$). The first power-law fit was realized in the range $t_s = 1$–$2.5\ \mu$m ($a = -0.77$ and $b = 0.46$), while the second power-law fit was realized in the range $t_s = 2.5$–$20\ \mu$m ($a = -0.51$ and $b = 3.78$).

In comparison, for a tape with the CFD architecture operating in the same conditions, the NZPV increases drastically as the stabilizer thickness decreases, ranging from $0.28\ \mathrm{m\,s^{-1}}$ when $t_s = 20\ \mu$m to $13.6\ \mathrm{m\,s^{-1}}$ when $t_s = 1\ \mu$m (blue squares in figure 5(b)). In that case, only one power-law curve was required to fit all data. The parameters used were $a = -1.30$ and $b = 13.41$ (dashed blue line).

In figure 5(c), the improvement ratio, namely the NZPV of a tape with the CFD architecture divided by the NZPV of a tape with the reference architecture, is given for the different stabilizer thicknesses (blue squares). The results indicate that, in terms of NZPV, the benefits of the CFD architecture increase as the stabilizer thickness decreases. For example, for $T = 77$ K, $I_c = 260$ A and $I_{op} = 0.9I_c$, the improvement ratio increases from 3.6 to 29 when t_s decreases from 20 to 1 μm. Two power-law functions were required to fit properly the data (dashed blue line). The parameters of the power-law fits were $a = -0.50$ and $b = 29.07$ ($t_s = 1$–$2.5\ \mu$m) and $a = -0.77$ and $b = 33.89$ ($t_s = 2.5$–$20\ \mu$m).

4.2. Effect of critical current

Manufacturers are currently putting a lot of efforts to increase the critical current of HTS tapes. This can be done either by increasing the critical current density of the HTS or by increasing its thickness. Therefore, we investigated the effect of an increased critical current density of the HTS layer on the NZPV of and tapes with the reference architecture and the CFD architecture. In figure 5, the NZPV of tapes having a critical current $I_c = 2I_c^* = 520$ A, where $I_c^* = 260$ A is used as a reference, are presented for $T_{op} = 77$ K and $I_{op} = 0.9I_c$.

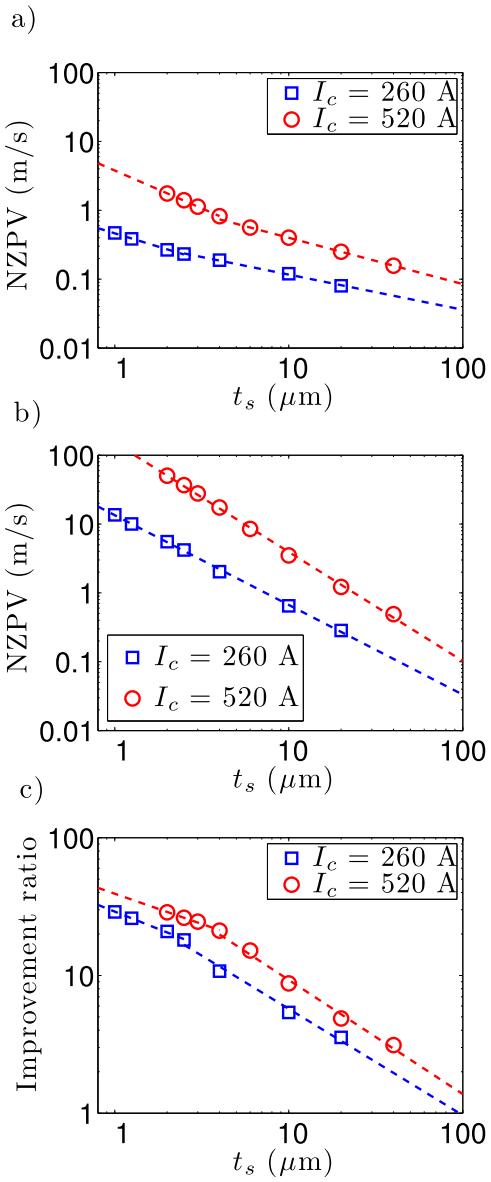

Figure 5. Influence of the stabilizer thickness on (a) the NZPV of a tape with the reference architecture, (b) the NZPV of a tape with the CFD architecture, and (c) the improvement ratio. Simulations were performed at $T = 77$ K, $I_{op} = 0.9I_c$ and $I_c = 260$ A (blue squares). Results for simulations performed using a critical current that is twice the original value ($T = 77$ K, $I_{op} = 0.9I_c$ and $I_c = 520$ A) are also presented (red circles). Dashed curves are fits of the data realized using a power-law model ($y = ax^b$).

We observe that, in both cases (reference and CFD), the NZPV increases when I_c increases (red circles in figures 5(a) and (b)). In the case of the reference architecture, two power-law functions were again required to properly fit the data (dashed red line). The first power-law fit was realized for the range $t_s = 2$–$4\ \mu$m ($a = -1.10$ and $b = 3.78$), while the second power-law fit was realized for the range $t_s = 4$–$40\ \mu$m ($a = -0.67$ and $b = 1.87$). In the case of the CFD architecture, it is interesting to note that the NZPV can reach values as high as $50.3\ \mathrm{m\,s^{-1}}$ when the stabilizer thickness is 2 μm, which is faster than any experimental NZPV value measured on 2G HTS CCs (modified or not) at

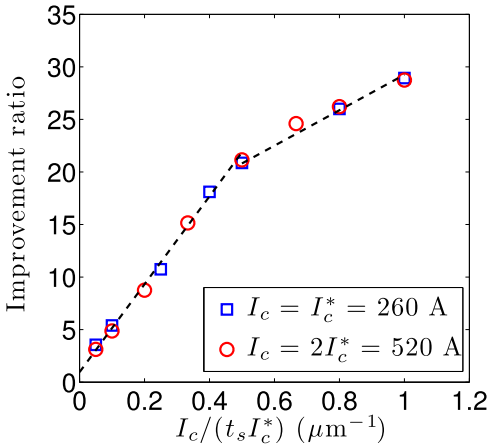

Figure 6. Dependence of the improvement ratio (figure 5(c)) with $I_c/(t_s I_c^*)$ for $I_c = I_c^* = 260$ A (blue squares) and $I_c = 2I_c^* = 520$ A (red circles). The dashed curves are linear fits of the data.

77 K [19]. The results could be well fitted using a single power-law curve ($a = -1.59$ and $b = 151.44$) (dashed red line). Finally, the improvement ratio when $I_c = 2I_c^*$ is presented in figure 5(c) (red circles). The parameters of the power-law fits (red dashed line) are $a = -0.44$ and $b = 39.20$ ($t_s =$ 2–4 μm) and $a = -0.83$ and $b = 62.48$ ($t_s =$ 4–40 μm).

In figure 6, the improvement ratio is plotted against $I_c/(t_s I_c^*)$. Interestingly, we notice that the data for both I_c values follow the same curve. At low $I_c/(t_s I_c^*)$ values (0–0.5 μm^{-1}), the improvement ratio increases linearly with $I_c/(t_s I_c^*)$ (slope = 41.8 μm, dashed curve). When $I_c/(t_s I_c^*) > 0.5$ μm^{-1}, the improvement ratio increases more slowly as $I_c/(t_s I_c^*)$ increases (slope = 16.9 μm). This is due to the faster increase of the NZPV of tapes with respect to the reference architecture as t_s reaches very small values.

4.3. Effect of operating temperature

The effect of the operating temperature on the NZPV was investigated for tapes having a 10 μm thick stabilizer layer. In figure 7(a), the NZPV is given for operating temperatures ranging from 10 to 77 K and $I_{op} = 0.9I_c$. We observe that, in both cases (reference and CFD), the NZPV increases as the operating temperature decreases. This can be attributed to many factors such as the strong reduction of the Hastelloy heat capacity and the increase of the critical current when the temperature decreases.

In figure 7(b), the improvement ratio is presented. We observe that, for a 10 μm thick stabilizer layer, the CFD architecture increases the NZPV by a factor of 6 when the temperature is between 60 and 70 K. At low temperatures (close to 10 K), the improvement ratio is reduced to a value of ≈ 4. Therefore, one can assert that the CFD architecture enhances the NZPV for the whole range of operating temperatures of 2G HTS CCs.

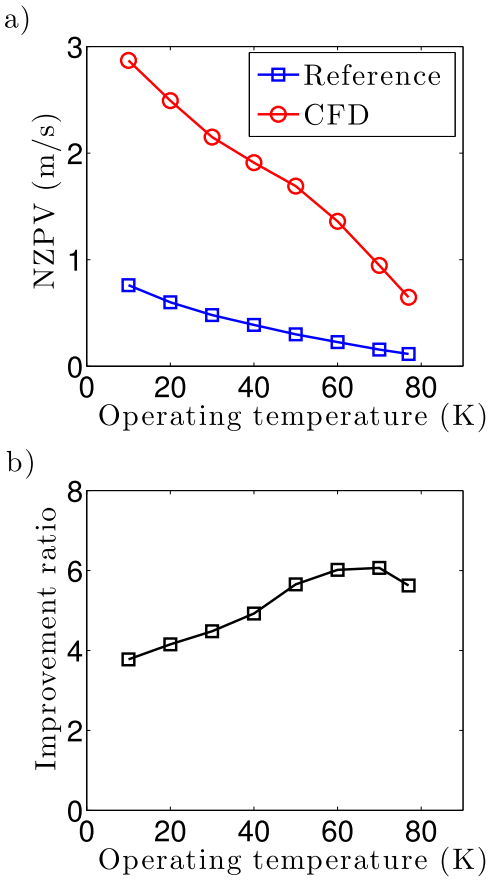

Figure 7. (a) Effect of the operating temperature on the NZPV of tapes having a 10 μm thick stabilizer layer ($I_{op} = 0.9I_c$) for the reference architecture and the CFD architecture. (b) Improvement ratio calculated from the NZPV values presented in (a).

5. Impact of the stabilizer geometry on the NZPV

In this section, the impact of the stabilizer geometry on the NZPV is investigated. More precisely, the influence of the stabilizer located on the substrate side is quantified. Two applications are targeted: superconducting coils for the generation of high magnetic field and SFCLs. Furthermore, the impact of the stabilizer located on the lateral sides of 2G HTS CCs is also studied.

5.1. Stabilizer located on the substrate side

We first investigated and quantified the influence on the NZPV of the thickness of the stabilizer layer located on the substrate side. From now on, to simplify the text, we will refer to the stabilizer layer located on the HTS side as 'HTS-side stabilizer', or simply 'HSS', and the stabilizer layer located on the substrate side as 'substrate-side stabilizer', or simply 'SSS'. The tape architecture used in the simulations is presented in figure 8, where the thickness of the stabilizer located on the lateral sides of the tape has been set equal to the thickness of the HSS (t_{HSS}). To simplify the simulations, the stabilizer is made solely of silver, even if in practice, one would use copper or other inexpensive metal. The total

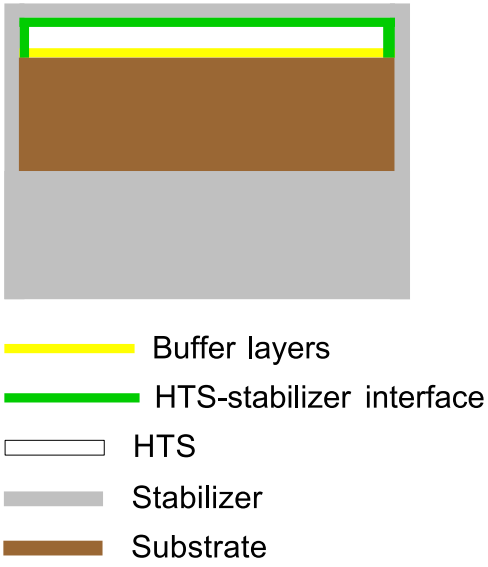

Figure 8. Cross-section view of a tape used to investigate the impact of the stabilizer thickness on the substrate side.

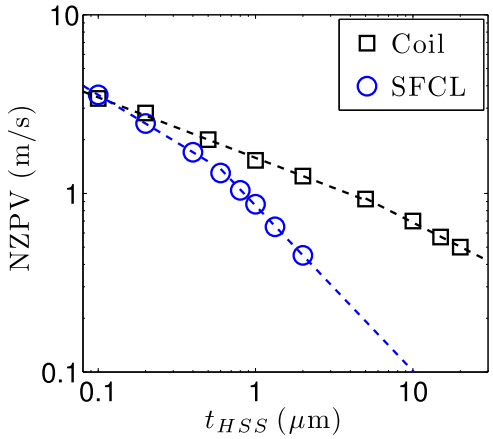

Figure 9. Dependence of the NZPV with the thickness of the stabilizer layer located on the HTS side (t_{HSS}) for the coil parameters ($T_{op} = 10$ K, $t_s = 20$ μm, $I_{op} = 0.9I_c$, $I_c = 800$ A) and the SFCL parameters ($T_{op} = 77$ K, $t_s = 2$ μm, $I_{op} = 0.9I_c$, $I_c = 260$ A). Dashed lines are fits of the data realized using power-law functions ($y = ax^b$).

thickness of stabilizer (t_s) corresponds to the sum of the thicknesses of the HSS and the SSS. For the coil application case, the following parameters were used: $t_s = 20$ μm, $T_{op} = 10$ K, $I_c = 800$ A and $I_{op} = 0.9I_c$ (720 A). For the SFCL application case, the following parameters were used: $t_s = 2$ μm, $T_{op} = 77$ K, $I_c = 260$ A and $I_{op} = 0.9I_c$ (234 A). In both cases, the resistance of the HTS-stabilizer interface was set to 1 $\mu\Omega\,\text{cm}^2$. The remaining simulation parameters are the same as those used before in this work (see tables 1 and 2).

Figure 9 presents the dependence of the NZPV with t_{HSS} for the two application cases. In both cases, we observe that the NZPV is much higher when most of the stabilizer is located on the substrate side. For the coil case, the NZPV equals 0.5 m s^{-1} when all stabilizer is located on the HTS side and increases up to 3.4 m s^{-1} when t_{HSS} is reduced to 0.1 μm (the thickness of the SSS (t_{SSS}) is then 19.9 μm). For the SFCL case, the NZPV equals 0.45 m s^{-1} when all stabilizer is located on the HTS side and increases up to 2.5 m s^{-1} when t_{HSS} is reduced to 0.2 μm (t_{SSS} is then 1.8 μm). The results could be well fitted using power-law functions ($y = ax^b$). For the coil case, the data could be well fitted using $a = -0.34$ and $b = 1.58$ ($t_{HSS} = 0.1$–5 μm) and $a = -0.45$ and $b = 1.93$ ($t_{HSS} = 5$–20 μm) (dashed black line). For the SFCL case, the data could be well fitted using $a = -0.53$ and $b = 1.04$ ($t_{HSS} = 0.1$–0.6 μm) and $a = -0.93$ and $b = 0.85$ ($t_{HSS} = 0.6$–2 μm) (dashed blue line).

Let us examine further the simulation results to obtain some insights on the mechanisms that explain the results presented in figure 9. We now focus on the tape with the coil parameters, i.e. $t_s = 20$ μm, $T_{op} = 10$ K, $I_c = 800$ A and $I_{op} = 0.9I_c$.

Figure 10(a) presents the temperature distribution in the HTS layer at a time $t = 5$ ms for a tape with 15 μm of HSS and 5 μm of SSS. We observe that the temperature gradient along the width of the tape is almost zero except at the edge of the tape (lower boundary), where the current is slightly more concentrated due to the presence of the lateral metallic stabilizer. On the other hand, we observe a sharp variation of the temperature at the normal zone boundary along the length of the tape. In figure 10(b), we present the temperature distribution in the HTS layer at a time $t = 5$ ms for a tape with 0.1 μm of HSS and 19.9 μm of SSS. We observe that the temperature gradient along the width of the tape is now stronger, especially at the edge of the tape, where the temperature increases drastically. Along the length of the tape, the variation in temperature is rather smooth before the normal zone suggesting that the generation of heat in front of the normal zone is done over a much longer distance than in the reference case. Also, we note that, when the HSS is thinner, the normal zone is bigger, indicating that the normal zone propagation is faster.

In figure 11, the current density in the SSS is illustrated for both cases. Moreover, we superposed red and blue arrows that represent the current density intensity and direction in the HTS layer and SSS respectively. In the case of the tape with 15 μm of stabilizer on the HTS side, we observe that the variation of the current density in the SSS along the length of the tape is quite sharp, indicating that the transfer of current from the HTS to the SSS occurs over a short length. Furthermore, we deduce, from the direction of the current in the HTS (red arrows), that most of the current transfers directly from the HTS to the HSS except at the edge of the tape where we observe that some current goes into the stabilizer located on the lateral sides in order to reach the SSS. In comparison, when almost all stabilizer is located on the substrate side, the variation of the current density in the SSS along the length of the tape is much smoother. This indicates that the current transfers from the HTS to the SSS over a considerable longer length. Also, the direction of the current in the HTS layer (red arrows) indicate that almost all current in the HTS goes through the stabilizer located on the lateral sides of the tape. This generates high Joule losses that explains the higher temperature observed at the edge of tape (see figure 10(b)).

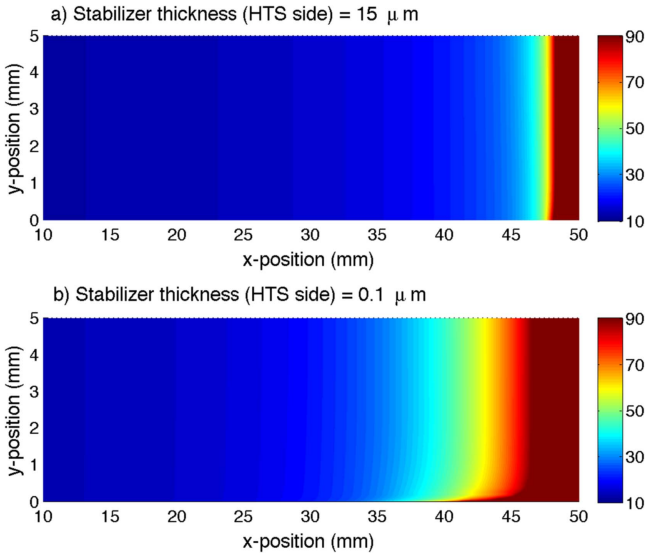

Figure 10. Two-dimensional distribution maps of the spatial distribution of the temperature in the middle of the HTS layer obtained at $t = 5$ ms for two tapes having 20 μm of stabilizer ($T_{op} = 10$ K, $I_c = 800$ A and $I_{op} = 0.9I_c$). The color bar (units: K) was adjusted to enhance the difference between the temperature distribution of the two tapes (saturation at 90 K). Only the bottom half-width of the tape is represented. In (a), the thickness of the stabilizer layer located on the HTS side is 15 μm (5 μm on the substrate side). In (b), the thickness of the stabilizer layer located on the HTS side is 0.1 μm (19.9 μm on the substrate side).

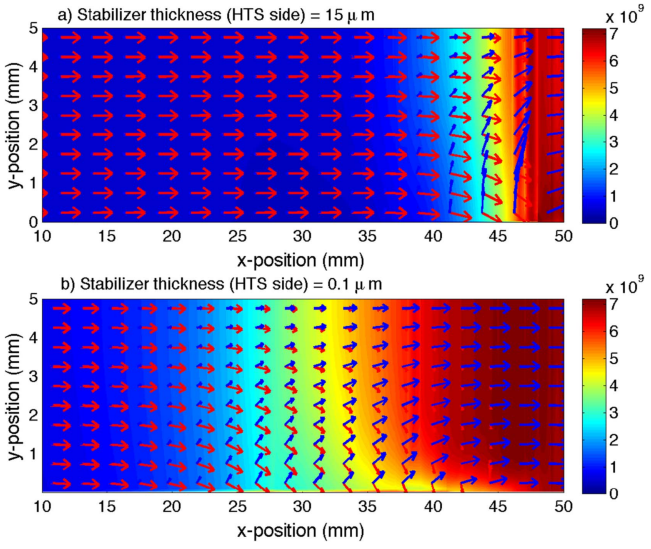

Figure 11. Two-dimensional distribution maps of the current density in the stabilizer layer located on the substrate side obtained at $t = 5$ ms for two tapes having 20 μm of stabilizer ($T_{op} = 10$ K, $I_c = 800$ A, $I_{op} = 0.9I_c$). The units of the color bar are A m^{-2}. The red and blue arrows represent the current density intensity and direction in the HTS and in the stabilizer located on the substrate side respectively. Only the bottom half-width of the tape is represented. In (a), the thickness of the stabilizer layer located on the HTS side is 15 μm (5 μm on the substrate side). In (b), the thickness of the stabilizer layer located on the HTS side is 0.1 μm (19.9 μm on the substrate side).

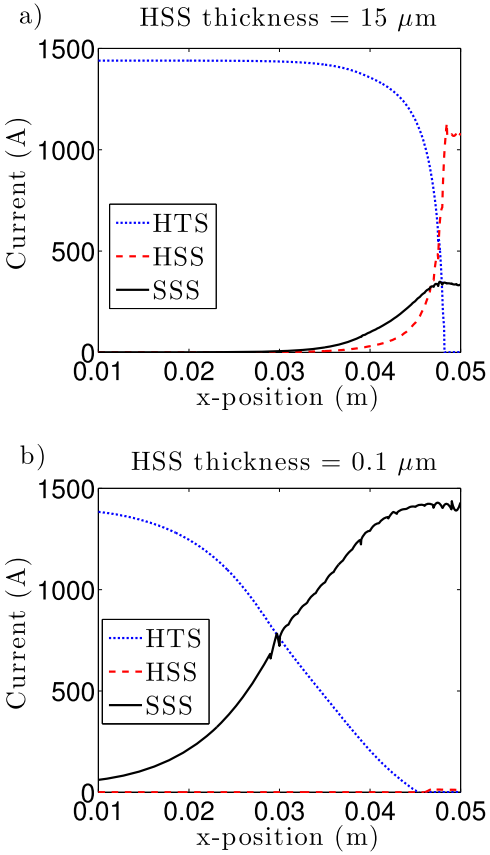

Figure 12. Total current at $t = 5$ ms along the length of the tape in the HTS layer and in the stabilizer located on (i) the HTS side and (ii) the substrate side, when t_{HSS} is (a) 15 μm and b) 0.1 μm.

The global current sharing between the HTS, the HSS and the SSS is presented in figure 12. In figure 12(a), where $t_{HSS} = 15$ μm, we observe that 90% of the total current in the HTS transfers to the stabilizer over a length of ≈6 mm. In comparison, when $t_{HSS} = 0.1$ μm (figure 12(b)), 90% of the total current in the HTS transfers to the stabilizer over a length of ≈28 mm, indicating that the CTL is larger. Basically, the CTL increases because the electrical resistance between the HTS and the SSS is higher than the electrical resistance between the HTS and the HSS. When $t_{HSS} = 0.1$ μm, one has to remember that because the resistance of the HSS is much higher than the resistance of the SSS, most of the current flows in the SSS upon the appearance of a normal zone.

Our results thus suggest that when the current transfers from the HTS to the SSS, the current concentrates in the stabilizer located on the lateral sides of the tape. As a consequence, this generates a local excess of heat on the edges of the tape, which increases the temperature at this location. This phenomenon is amplified as the volume fraction of SSS is increased. Furthermore, our results indicate that the CTL is increased as the volume fraction of SSS is increased. This implies that the local excess of heat is generated over a longer distance in front of the normal zone, which accelerates the normal zone propagation [16]. This type of effect was previously observed for tapes with the CFD architecture (see [18]).

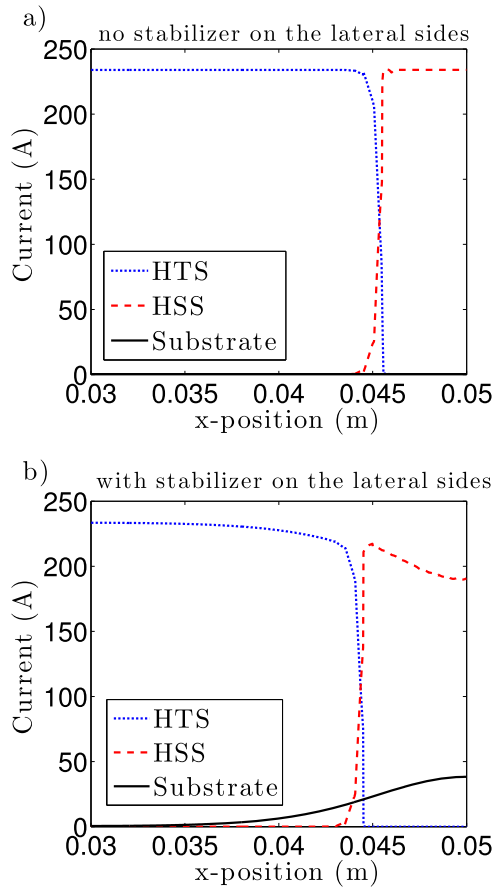

Figure 13. Total current at $t = 20$ ms along the length of the tape for the HTS, stabilizer (HTS side) and substrate when (a) there is no stabilizer on the lateral sides and (b) when stabilizer is present on the lateral sides. The parameters used for these simulations were $T_{op} = 77$ K, $t_s = 2$ μm, $I_c = 260$ A and $I_{op} = 0.9I_c$.

Finally, it is worth mentioning that the impact of the stabilizer geometry on the stability of 2G HTS CCs has been investigated earlier by Levin *et al* through numerical simulations [24]. However, the effects of the stabilizer geometry on the NZPV was not addressed. Nevertheless, Levin *et al* concluded that putting all stabilizer on the HTS side ensured the maximum of stability. On the other hand, our results demonstrate that putting most of the stabilizer on the substrate side maximizes the NZPV. This is in agreement with previous published works, i.e. there is a compromise to be made between the stability and the NZPV [3, 18, 25].

5.2. Stabilizer located on the lateral sides

We also investigated the effect on the CTL and NZPV of the stabilizer located on the lateral sides of a tape. For this investigation, we considered the 'SFCL' case ($t_s = 2$ μm, $T_{op} = 77$ K, $I_c = 260$ A and $I_{op} = 0.9I_c$), where all the stabilizer was put on the HTS side of the tape.

Simulations were performed for two different cases. In the first case (figure 13(a)), the tape has no stabilizer on the lateral sides while in the second case (figure 13(b)), the tape has a 2 μm thick stabilizer on the lateral sides. In both cases, when the current transfers from the HTS to the stabilizer, we observe that the CTL is quite small (less than 1 mm). In the first case (no stabilizer on the lateral sides), the totality of the current is transferred from the HTS to the stabilizer. No current flows in the substrate since the HTS is not electrically connected to the substrate. In the second case (with stabilizer on the lateral sides), approximately 84% of the total current is transferred to the stabilizer and the rest of the current (≈16%) flows in the substrate. However, when current transfers from the HTS to the substrate, the CTL is much longer (≈9 mm). Furthermore, a NZPV of 0.27 m s^{-1} is obtained when no stabilizer is present on the lateral sides while a value of 0.45 m s^{-1} is obtained when stabilizer is present on the lateral sides.

These results show that enhanced CTL and NZPV can be obtained even if no stabilizer is present on the substrate side but present on the lateral sides of the tape. This is due to the fact that a significant amount of current will transfer into the substrate upon the appearance of a normal zone. The condition to observe this effect is to ensure that the electrical conductance of the substrate is not negligible in comparison with that of the stabilizer.

6. Concluding remarks

The simulations results presented in this paper allowed us to draw the followings conclusions on the CFD concept, which was first introduced in [18]: (i) the CFD becomes more and more effective as the total thickness of stabilizer becomes smaller and as the critical current becomes larger, and (ii) the CFD increases the NZPV for the whole operating temperature range of 2G HTS CCs. Therefore, we can assert that the CFD concept is definitely an asset for most applications using HTS tapes with a thin stabilizer, such as SFCLs. In applications requiring thicker stabilizer, such as HTS magnets, the CFD concept also provides benefits, although less pronounced.

Investigation on the stabilizer geometry has revealed that the NZPV of 2G HTS CCs with thick stabilizer can be significantly enhanced if the stabilizer layer on the substrate side is much thicker than the stabilizer layer on the HTS side. Note that this is only true if stabilizer is also present on the lateral sides of the tape to ensure an electrical connection between the HTS and the stabilizer located on the substrate side. It is useful to reiterate that the key element in the original CFD concept is to deliberately increase the length of the path the current must take when it transfers from the HTS to the stabilizer upon a quench, which is called the CTL [18]. As a consequence, the region in front of the normal zone, where the Joule losses are generated, is longer, which accelerates the normal zone propagation. In this work, the same effect was created by choosing the proper stabilizer geometry in place of inserting a high resistance layer at the HTS–stabilizer interface, as done in the classical CFD concept. In other words, we can say that the buffer layers act as a CFD, similarly to the high resistance layer inserted at the HTS–stabilizer interface in the classical CFD concept. When having the proper stabilizer geometry, one can constrain the current to flow around the buffer layers upon a quench, which in turn increases the CTL and the NZPV, even in the case of tapes having a thick

stabilizer. This result is particularly interesting in the case of coil applications, since a thick stabilizer allows the tape to sustain a high current during a considerable amount of time after quenching. It is worth mentioning that the adiabatic condition used in this paper (no thermal exchange with the surrounding environment) will probably not be a good assumption in real-life applications, which may lead to different values of NZPV than those calculated in this work. Heat exchange of HTS tape with the surrounding environment is highly dependent on the application and will have to be dealt with on a case-by-case basis.

Furthermore, we have shown that even if no stabilizer is present on the substrate side, a longer CTL and faster normal zone propagation can be observed if the electrical conductance of the substrate is not negligible in comparison with that of the HSS. The key element to observe this effect is the presence of stabilizer on the lateral sides of the tape in order to electrically connect the HTS to the metallic substrate.

Acknowledgments

This work was supported by research grants from NSERC (Canada) and FRQNT (Québec).

References

[1] Wang X, Trociewitz U P and Schwartz J 2009 Self-field quench behaviour of $YBa_2Cu_3O_7$ coated conductors with different stabilizers *Supercond. Sci. Technol.* **22** 085005

[2] Grabovickic R, Lue J W, Gouge M J, Demko J A and Duckworth R C 2003 Measurements of temperature dependence of the stability and quench propagation of a 20 cm long RABiTS Y–Ba–Cu–O tape *IEEE Trans. Appl. Supercond.* **13** 1726

[3] Wang X, Trociewitz U P and Schwartz J 2007 Near-adiabatic quench experiments on short $YBa_2Cu_3O_{7-\delta}$ coated conductors *J. Appl. Phys.* **101** 053904

[4] Roy F, Dutoit B and Sirois F 2010 Quench nucleation obtained by local reduction of I_c in coated conductors *J. Phys.: Conf. Ser.* **234** 032050

[5] Celentano G *et al* 2009 Hot spot stimulated transition in YBCO coated conductors: experiments and simulations *IEEE Trans. Appl. Supercond.* **19** 2486

[6] Pelegrin J, Martinez E, Angurel L A, Xie Y-Y and Selvamanickam V 2011 Numerical and experimental analysis of normal zone propagation on 2G HTS wires *IEEE Trans. Appl. Supercond.* **21** 3041

[7] Chan W K, Masson P J, Luongo C and Schwartz J 2010 Three-dimensional micrometer-scale modeling of quenching in high-aspect-ratio coated conductor tapes: I. Model development and validation *IEEE Trans. Appl. Supercond.* **20** 2370

[8] Chan W K and Schwartz J 2011 Three-dimensional micrometer-scale modeling of quenching in high-aspect-ratio coated conductor tapes: II. Influence of geometric and material properties and implications for conductor engineering and magnet design *IEEE Trans. Appl. Supercond.* **21** 3628

[9] Badel A, Antognazza L, Therasse M, Abplanalp M, Schacherer C and Decroux M 2012 Hybrid model of quench propagation in coated conductors for fault current limiters *Supercond. Sci. Technol.* **25** 095015

[10] Casali M, Breschi M and Ribani P L 2015 Two-dimensional anisotropic model of YBCO coated conductors *IEEE Trans. Appl. Supercond.* **25** 6600112

[11] Bonura M and Senatore C 2016 An equation for the quench propagation velocity valid for high field magnet use of REBCO coated conductors *Appl. Phys. Lett.* **108** 242602

[12] Markiewicz W D *et al* 2012 Design of a superconducting 32 T magnet with REBCO high field coils *IEEE Trans. Appl. Supercond.* **22** 4300704

[13] Colangelo D and Dutoit B 2012 Inhomogeneity effects in HTS coated conductors used as resistive FCLs in medium voltage grids *Supercond. Sci. Technol.* **25** 095005

[14] Senatore C, Alessandrini M, Lucarelli A, Tediosi R, Uglietti D and Iwasa Y 2014 Progresses and challenges in the development of high-field solenoidal magnets based on RE123 coated conductors *Supercond. Sci. Technol.* **27** 103001

[15] Colangelo D and Dutoit B 2014 Analysis of the influence of the normal zone propagation velocity on the design of resistive fault current limiters *Supercond. Sci. Technol.* **27** 124005

[16] Levin G A, Novak K A and Barnes P N 2010 The effects of superconductor-stabilizer interfacial resistance on the quench of a current-carrying coated conductor *Supercond. Sci. Technol.* **23** 014021

[17] Lacroix C, Fournier-Lupien J-H, McMeekin K and Sirois F 2013 Normal zone propagation velocity in 2G HTS coated conductor with high interfacial resistance *IEEE Trans. Appl. Supercond.* **23** 4701605

[18] Lacroix C and Sirois F 2014 Concept of a current flow diverter for accelerating the normal zone propagation velocity in 2G HTS coated conductors *Supercond. Sci. Technol.* **27** 035003

[19] Lacroix C, Lapierre Y, Coulombe C and Sirois F 2014 High normal zone propagation velocity in second generation high-temperature superconductor coated conductors with a current flow diverter architecture *Supercond. Sci. Technol.* **27** 055013

[20] Ekin J W 2006 *Experimental Techniques for Low-Temperature Measurements* (Oxford: Oxford University Press)

[21] Lacroix C, Sirois F, Slimani K and Cave J 2013 Electro-thermal response of 2G HTS coated conductors subjected to current pulses *IEEE Trans. Appl. Supercond.* **23** 6601605

[22] Falorio I, Young E A and Yang Y 2014 Flux pinning distribution and E–J characteristics of 2G YBCO tapes *J. Phys.: Conf. Ser.* **507** 022004

[23] Bonnard C-H, Sirois F, Lacroix C and Didier G 2017 Multi-scale model of resistive-type superconducting fault current limiters based on 2G HTS coated conductors *Supercond. Sci. Technol.* **30** 014005

[24] Levin G A, Barnes P N and Bulmer J S 2007 Current sharing between superconducting film and normal metal *Supercond. Sci. Technol.* **20** 757

[25] Dresner L 2002 *Stability of Superconductors* (New York: Springer)